# Journal of Materials Chemistry A

Accepted Manuscript


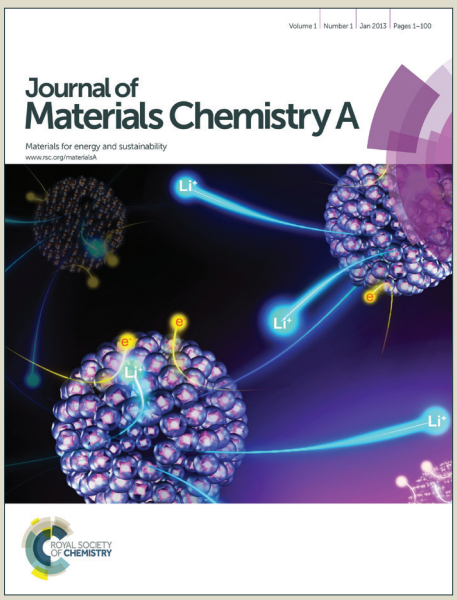





ROYAL SOCIETY OF CHEMISTRY

www.rsc.org/materialsA

# Enhancing Visible-Light Photoelectrochemical Water Splitting through Transition-Metal Doped $TiO_2$ Nanorod Arrays

Chengzhi Wang[1], Zhuo Chen[*1], Haibo Jin[*1], Chuanbao Cao[1], Jingbo Li[1] and Zetian Mi[2]

[1]Department of Materials Physics and Chemistry, School of Materials Science and Engineering, Beijing Institute of Technology, Beijing 100081, People's Republic of China

[2]Department of Electrical and Computer Engineering, McGill University, 3480 University Street, Montreal, Quebec H3A 0E9, Canada

## Abstract

Extending the photoresponse from the ultraviolet (UV) to the visible light region while maintaining a high photocatalytic activity has been an important challenge for $TiO_2$. We demonstrate the use of transition-metal doping treatment as a facile and effective strategy to substantially improve the performance of $TiO_2$ nanorods in the visible light region for photoelectrochemical (PEC) water splitting. The effect of Fe, Mn and Co as dopants on the PEC performance of the $TiO_2$ nanorods was investigated, wherein the Fe doping is the most effective route to enhance the photoactivity of $TiO_2$. The photocurrent density of Fe-$TiO_2$ sample increases significantly with bias voltage and reaches 2.92 mA/cm$^2$ at 1.25 V vs. RHE, which are five times higher than that of the undoped $TiO_2$. Even under visible light illumination (>420 nm), the photocurrent density of Fe-$TiO_2$ is as high as 0.96 mA/cm$^2$ at 1.25 V vs. RHE. Incident-photon-to-current-conversion (IPCE) efficiency (up to ~ 18%) measurements reveal that the Fe-$TiO_2$ nanorod sample significantly

improve the photoresponse not only in the UV region but also in the visible light region. Fe doping not only enhances the visible light absorption of $TiO_2$ nanorods by creating impurity states near the conduction band, but also obviously increases carrier density of $TiO_2$, leading to effective carrier separation and transportation and relatively long electron lifetime. Due to their relatively high photocatalytic activity, the Fe-$TiO_2$ nanorods can serve as a promising candidate for various areas, such as solar water splitting, dye-sensitized solar cells, and photocatalysis.

## 1. Introduction

Photocatalytic hydrogen generation by water splitting has attracted extensive research interest in the past decade because of the increasing concern on energy and environmental issues.[1-21] The photocatalytic water-splitting systems can be classified into two main categories: suspended photocatalysts and photoelectrochemical (PEC) cells. Since Fujishima and Honda reported on the photoelectrolysis of water into hydrogen and oxygen on a $TiO_2$ photoelectrode,[22] semiconductor-based PEC water splitting by solar energy has been regarded as one of the most important ways for hydrogen generation.[2,9] Generally, realizing the PEC water splitting requires the semiconductor to meet the following property criteria: stability, appropriate band gap, efficient visible light absorption,

and suitable band-edge positions to straddle the water redox potentials. Since most of narrow gap semiconductors suffer from photo-corrosion, photocatalytic materials still are limited to a few wide band gap oxide semiconductors such as $TiO_2$[10,14,17,18], $SrTiO_3$[10], and $WO_3$[10]. Among various wide band gap semiconductors, $TiO_2$ is one of the most promising materials due to its low cost, good photocatalytic activity, and chemical stability.[10] However, the efficiency of solar PEC water splitting based on $TiO_2$ is very low due to its wide band gap，resulting in response only under UV light. Numerous approaches have been developed to enhance the visible light response of $TiO_2$, such as metal or non-metal doping, quantum dot or dye sensitization, composite semiconductors and so on.[23] Hereinto, doping serves as an effective route in the modifications of $TiO_2$ because it can keep the integrity of the crystal structure and make favorable changes in the electronic structure. Up to now a great deal of theoretical and experimental efforts have been devoted to 3d transition-metal (TM) doped $TiO_2$.[23,24] Theoretical researches predict that the formation of new states closed to the valence band and conduction band induced by 3d TM dopants results in significant energy gap narrowing together with enhanced optical absorption.[24,25] However, many experimental reports indicate that the effect of red shift by 3d TM dopants is not obvious, and these dopants in $TiO_2$ will act as recombination centers, which result in the limited enhancement of photocatalytic activity

or even lower than pure $TiO_2$.[23, 26-30] Until recently, to improve the visible light absorption while maintaining a high photocatalytic activity has been challenging.

Additionally, the photocatalytic performance of $TiO_2$ can be improved by rationally controlling its morphology and orientation etc.[31-38] For example, vertically aligned $TiO_2$ nanorod arrays as photoanode not only provide large surface area and efficient light trapping, but also have short diffusion distance for photogenerated minority carriers, which is expected to facilitate the charge separation and reduce the loss due to electron-hole recombination.[33] Recently, considerable efforts have been devoted to growing various oriented $TiO_2$ nanostructures and modifying their properties, such as oriented single-crystalline rutile $TiO_2$ nanorods[39] or nanowires,[31,35] hydrogen-treated $TiO_2$ nanowires,[33] Sn doped $TiO_2$ nanowires,[34] branched $TiO_2$ nanorods,[36] and W doped $TiO_2$ nanowires etc.[38] However, most of these efforts only improve the PEC performance of $TiO_2$ nanowires in the UV region, and the improvement in the visible light region is very limited. For example, the IPCE values of H:$TiO_2$ and H, N-$TiO_2$ nanowires are below 0.7% from 440 nm to 650 nm[33] and 4% from 420 nm to 550 nm,[32] respectively. To our knowledge, there have been no reports on the 3d-TM doped $TiO_2$ nanorod arrays with both improved PEC performance and strong visible light response.

Here, we demonstrate that a significant improvement of the PEC water

splitting activity under visible light irradiation based on $TiO_2$ nanorod arrays can be achieved by doping 3d TM using a facile solution method. The PEC performance of the TM doped $TiO_2$ nanorods can further be adjusted by the concentration of TM ion in the solution. The effect of Fe, Mn and Co as dopants on the PEC performance of $TiO_2$ nanorods was investigated in which Fe doping is the most effective route to enhance the photoactivity of $TiO_2$. The photocurrent density of Fe-$TiO_2$ sample increases significantly with bias voltage and reaches 2.92 mA/cm$^2$ at 1.25 V vs. RHE, which is five times higher than that of the undoped $TiO_2$. Even under visible light illumination (>420 nm), the photocurrent density of Fe-$TiO_2$ is as high as 0.96 mA/cm$^2$ at 1.25 V vs. RHE. Incident-photon-to-current-conversion efficiency (IPCE) (up to ~ 18%) indicates that Fe doped $TiO_2$ nanorod arrays show substantially enhanced photoresponse not only in the UV region but also in the visible light region in comparison to the undoped $TiO_2$ nanorod sample, and exhibit long-term stability. The transition-metal doping hydrothermal treatment we developed is a facile and effective strategy to substantially improve the performance of $TiO_2$ nanorods for photoelectrochemical (PEC) water splitting. The relatively high PEC performance of the Fe-$TiO_2$ nanorods opens new opportunities in various areas, such as solar water splitting, dye-sensitized solar cells, and photocatalysis.

## 2. Experimental section

$TiO_2$ nanorod arrays on a fluorine-doped tin oxide (FTO) glass substrate were grown by a hydrothermal method previously reported by Liu et al.[39] For doping TM in $TiO_2$, 1g of urea and 10-100 mM TM nitrate were dissolved in 15 mL aqueous solution. The solution and the FTO substrate with $TiO_2$ nanorod arrays were transferred to a 20mL Teflon-lined stainless steel autoclave. The autoclave was sealed and put into an electric oven at 150 $^oC$ for 2 h. When the autoclave was cooled down to room temperature, these samples were cleaned with deionized water and were dried in air. The colors of the samples were obviously different than that of $TiO_2$ nanorod arrays without dopants, and depended on the doping metal ion. Finally the samples were annealed in a furnace at 450 $^oC$ for 30 min.

The morphologies and structures of the samples were characterized by X-ray diffraction (XRD, Philips X'pert Pro diffractometer), field-emission scanning electron microscope (FESEM, Hitachi S-4800), energy dispersive X-Ray spectrometry (EDS), X-ray photoelectron spectroscopy (XPS, PerkinElmer Physics PHI 5300), and field-emission transmission electron microscope (HRTEM, Tecnai F20). For TEM analysis, samples were prepared by scratching off nanorod flakes on a Ni

grid.

The photoelectrochemical measurement was performed in 1 M KOH solution using a three-electrode configuration. $TiO_2$ nanorod arrays with or without 3d TM dopants were used as the working electrodes (photoanodes), saturated Ag/AgCl as the reference electrode, and a platinum foil as a counter electrode. The photocurrent measurements were carried out by applying an external bias to the cell using an electrochemical station (Zahner IM6e, Germany) with a scan rate of 10 mV/s and using a 150 W Xe solar simulator (Newport 94021A) with AM 1.5G filter as light source. Incident-photon-to-current-conversion efficiency (IPCE) spectra were measured on a QE/IPCE Measurement Kit (Crowntech QTest Station 1000AD) with a tungsten halogen lamp (CT-TH-150), a calibrated silicon diode and a monochromator (Crowntech QEM24-S 1/4 m).

## 3. Results and Discussion

The TM-doped $TiO_2$ nanorod arrays on FTO were prepared using a hydrothermal method. After the doping treatment, the color of the samples will change from gray-white (for pure $TiO_2$) to light red (for Fe doped $TiO_2$ denoted by Fe-$TiO_2$), brown-red (for Mn doped $TiO_2$ denoted by Mn-$TiO_2$) and yellow (for Co doped $TiO_2$ denoted by Co-$TiO_2$), respectively, as shown in Figure 1. SEM images reveal that vertically or

slantingly aligned nanorod arrays were uniformly grown in high density on the FTO substrate (Figure 1). These nanorods are uniform with a rectangular cross section. The nanorod diameters are in the range of 50-300 nm and the typical nanorod lengths are around 5 μm. There are no obvious changes in morphology by comparing with SEM images of the samples before and after doping. From the insets in Figure 1, it can be seen that the color is uniform, implying uniform distribution of dopants in the $TiO_2$ nanorods. The EDS results of the TM-$TiO_2$ nanorods are shown in Table S1(see supporting information).

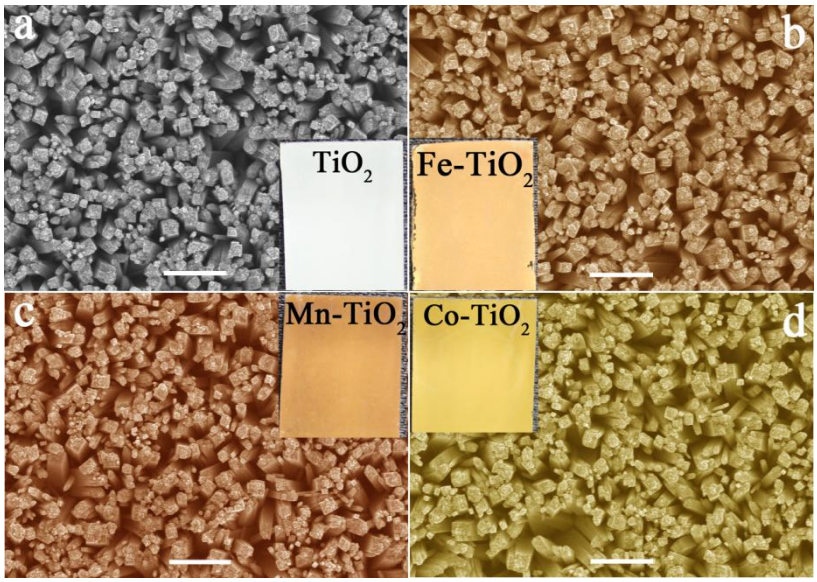


Figure 1. SEM images of (a) $TiO_2$, (b) Fe-$TiO_2$, (c) Mn-$TiO_2$ and (d) Co-$TiO_2$ nanorod arrays on FTO substrates. Insets are the corresponding digital pictures, respectively. All scale bar are 1μm.

To investigate the effect of doping on the crystal structure, XRD spectra were collected from the $TiO_2$ nanorods and TM doped $TiO_2$ nanorods grown at various metal salt concentrations (50mM for Fe- and Mn-$TiO_2$, 10mM for Co-$TiO_2$), as shown in Figure 2. If no special explanation, all the following samples were prepared under these conditions. All the XRD

patterns have two diffraction peaks at 2θ angles of 36.5 °and 63.2 °, which can be indexed as the (101) and (002) reflection of tetragonal rutile $TiO_2$ (JCPDS No. 88-1175). The (002) diffraction peak dominating over the (101) peak indicates that the nanorods grew preferentially along the <001> direction. Other peaks can be contributed to the FTO substrate. Obviously, there is no impurity peak after doping. The decrease of the (002) peak intensity depends on the doping metal element in which the most decrease is Co, the second for Mn and the least for Fe. These decreases may be due to the increase of defect density in $TiO_2$ structures, which has also been observed in the hydrogen-treated $TiO_2$ nanowire arrays[33].

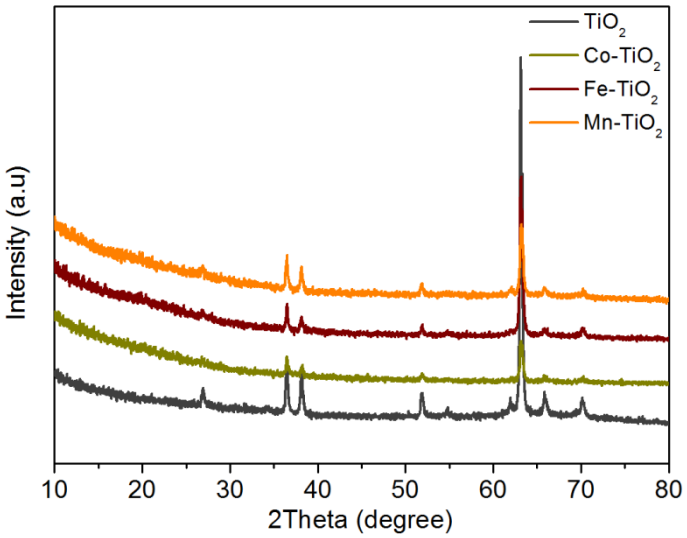


Figure 2. XRD spectra of $TiO_2$ (graw cruve), Co-$TiO_2$ (green-yellow cruve), Fe-$TiO_2$ (wine cruve) and Mn-$TiO_2$(orange cruve) nanorod arrays on FTO substrates.

Structural characterizations of the TM-doped $TiO_2$ nanorods were performed by TEM and HRTEM. Figure 3a shows a TEM image of the Fe-$TiO_2$ nanorod. Basically, the diameters of the nanorods under TEM

observation are consistent with the SEM results. The HRTEM image shown in Figure 3b reveals the single-crystalline structure of the nanorod, and gives a lattice fringe of about 0.32 nm, corresponding to the $d_{110}$ space of the bulk rutile $TiO_2$. The dopant distribution in the nanorod was further analyzed by EDS. Variations of the O Lα, Ti Lα,Ti Kα, Fe Lα and Fe Kα signals along the nanorod are given in Figure 3c. Clearly, the distribution of Fe element along the nanorod axial and radial direction is uniform. The analysis of EDS mapping was also applied to Mn- and Co-$TiO_2$ nanorods, which confirm that the distribution of Mn and Co in nanorods is also uniform (see Figure S1 and S2 in Supporting Information).

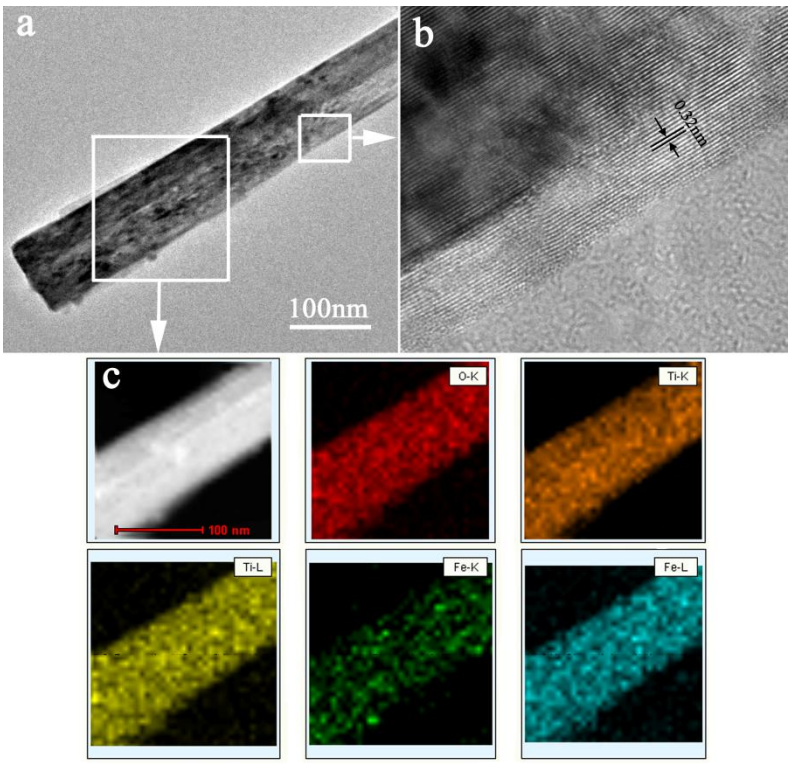


Figure 3. (a) TEM, (b) HRTEM and (c) EDS mapping images of single Fe-$TiO_2$ nanorod.

XPS was employed to explore the chemical states of surface elements of the 3d-TM doped $TiO_2$ nanorod arrays. Two peaks at 464.3 and 458.5 eV were observed from the fully scanned $TiO_2$ spectrum (Figure 4a), which can be assigned to Ti $2p_{1/2}$ and Ti $2p_{3/2}$ spin-orbital components in $TiO_2$, respectively.[40,41] After the doping treatments, the high-resolution Mn, Fe and Co 2p XPS spectra of the samples are shown in Figures 4b,4c and 4d, respectively. Figure 4b shows the Mn 2p core-level XPS spectrum with two peaks at 653.5 (Mn $2p_{1/2}$) and 641.6 eV (Mn $2p_{3/2}$). The binding energies of Mn 2p are consistent with that of $Mn_2O_3$.[42] The Fe 2p XPS spectrum is identical with Fe $2p_{1/2}$ and $2p_{3/2}$ peaks centered at binding energies of 724.4 and 710.6 eV, which are consistent with the typical values for $Fe_2O_3$.[43] In the Co 2p spectrum (Figure 4d), the doublet peaks at 796.6 and 780.2 eV could be indexed to Co $2p_{1/2}$ and Co $2p_{3/2}$, respectively. The peaks could be assigned to the bivalent cobalt corresponding to the standard CoO.[44,45] The above results clearly indicate that Mn, Fe and Co have been successfully incorporated into the $TiO_2$ nanorods.

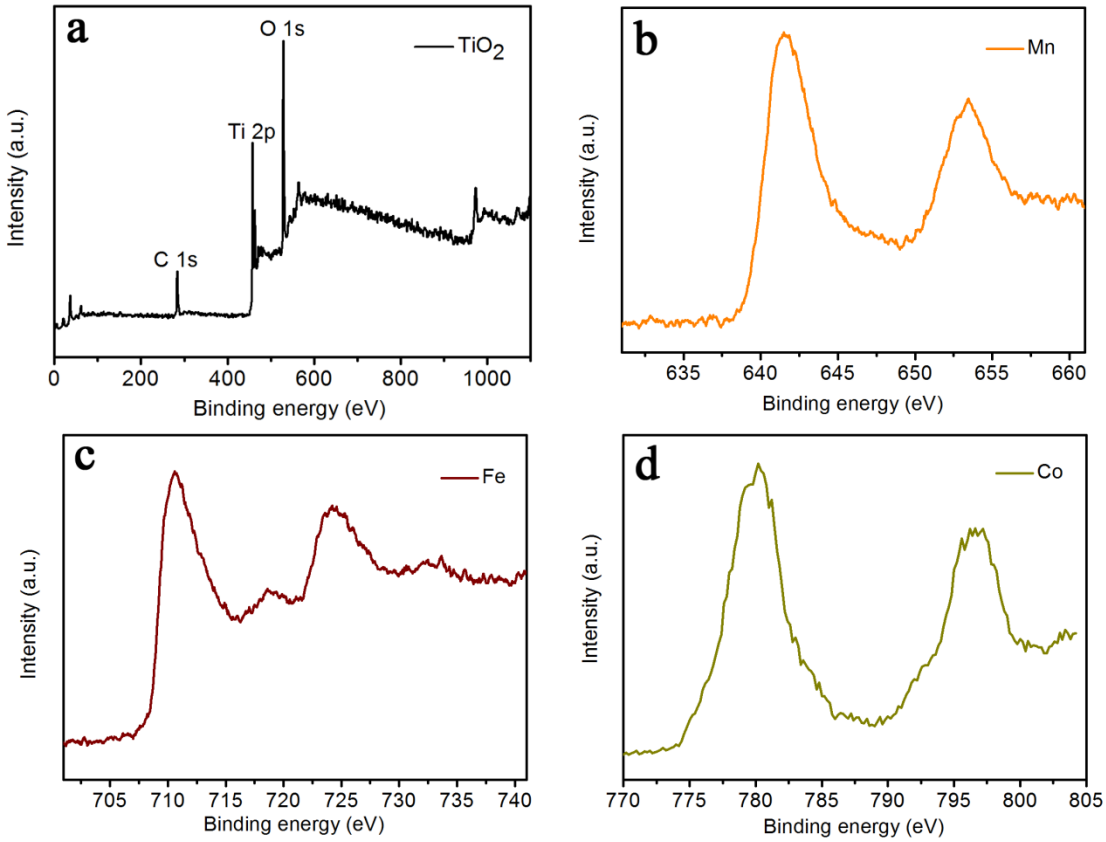


Figure 4. (a) XPS spectra of $TiO_2$ nanorod and high-resolution (b) Mn, (c) Fe and (d) Co 2p core-level XPS spectra of the $TiO_2$ nanorod doped with Mn, Fe and Co, respectively.

To evaluate the effect of dopants on the PEC properties of $TiO_2$, we measured the photocurrents of colored Fe-, Mn- and Co-$TiO_2$ nanorod photoanodes and compared them with those of the undoped $TiO_2$ nanorods. All $TiO_2$ nanorod samples were fabricated into photoanodes with a well-defined area of 0.2 $cm^2$. The PEC measurements were conducted in 1 M KOH electrolyte (pH = 13.5), under simulated sunlight illumination at 100 $mW/cm^2$ from a 150 W xenon lamp coupled with an AM 1.5G filter. The linear sweeps of $TiO_2$ (gray) and $TiO_2$ nanorods doped with Fe (wine), Mn (orange), and Co (green-yellow), in a potential range of 0 to 1.75 V vs RHE, are shown in Figure 5a. It is seen that the

dark current densities are essentially negligible (3-7 μA/cm$^2$) even at high potentials of 1.75 V vs RHE. The photocurrent densities increase significantly with bias voltage and reach 0.76 mA/cm$^2$ for Co-$TiO_2$, 1.25 mA/cm$^2$ for Mn-$TiO_2$ and 2.92 mA/cm$^2$ for Fe-$TiO_2$ at 1.25 V vs RHE, which are two and five times higher than the photocurrent density of 0.56 mA/cm$^2$ for the undoped $TiO_2$, respectively, except a slight increase for Co-$TiO_2$. It is obvious that Fe doping by a simple hydrothermal method greatly improves the PEC properties of $TiO_2$ and yields a maximum photocurrent density of 2.92 mA/cm$^2$ at 1.25 V vs RHE. This value is slightly better than the best reported values of 2.8 mA/cm$^2$ for $TiO_2$ photoanodes[46], 2.5 mA/cm$^2$ at 1.23V vs RHE for hydrogen-treated $TiO_2$ nanowire arrays[33] and 2.0 mA/cm$^2$ at 1.65V vs RHE for Ti-Fe-O nanotube arrays.[37] The $TiO_2$, Mn-$TiO_2$ and Fe-$TiO_2$ samples exhibit an obvious increase in photocurrent density at an onset potential of 0.25 V vs RHE and reach their saturated photocurrents at a low potential of 0.6 V vs RHE, except that the photocurrent density of Co-$TiO_2$ sample increases near-linearly with the applied potential and doesn't reach saturation at the scanning voltage range.

To test the photoresponse of TM-doped $TiO_2$ samples in the visible light region, photocurrents were measured with the use of a 420 nm long-pass filter, as shown in Figure 5b. The onset potentials for the four samples positively shift to 0.36 V vs RHE due to the decrease of the

photogenerated carrier. The photocurrent densities of TM-doped $TiO_2$ samples are higher than that of $TiO_2$ (gray). Under visible light illumination, the photocurrent density of Fe-$TiO_2$ is as high as 0.96 $mA/cm^2$ at 1.25 V vs RHE. For Mn- and Co-$TiO_2$, the photocurrent densities are 0.34 and 0.14 $mA/cm^2$ at 1.25 V vs RHE, respectively. These results indicate that in this case Fe doping is an effective method to promote the PEC performance of $TiO_2$ in the visible light region. However, the enhancement induced by Co doping is relatively limited, which probably results from the increase of defect density supported by XRD data. For enhancing photocatalytic activity, effective carrier transfer to the catalyst/solution interface is another important factor, in addition to broad and strong optical absorption. Only if the electron and hole excited by photon are transferred to the surface, photocatalytic reactions could occur. In case of doping, metal ions could enhance optical absorption, but they likely behave as recombination centers, which would hinder electron/hole transferring to the surface. Therefore, there exists an optimum concentration of doped metal ion, below which the improvement of optical absorption is negligible, and above which the photocatalytic activity decreases due to the increase in recombination. Figure 5c shows the photocurrent densities of Fe-, Mn- and Co-$TiO_2$ nanorod arrays at 1.25 V vs Ag/AgCl as a function of metal ion concentration. The Fe- and Mn-$TiO_2$ nanorod arrays prepared using

50mM $Fe(NO_3)_3$ and $Mn(NO_3)_2$ solutions, respectively, yield a maximum photocurrent density. The photocurrent density of Co-$TiO_2$ nanorod arrays decreases as the Co ion concentration increases. By optimizing the metal ion concentration, the condition for maximum photocurrent density was obtained.

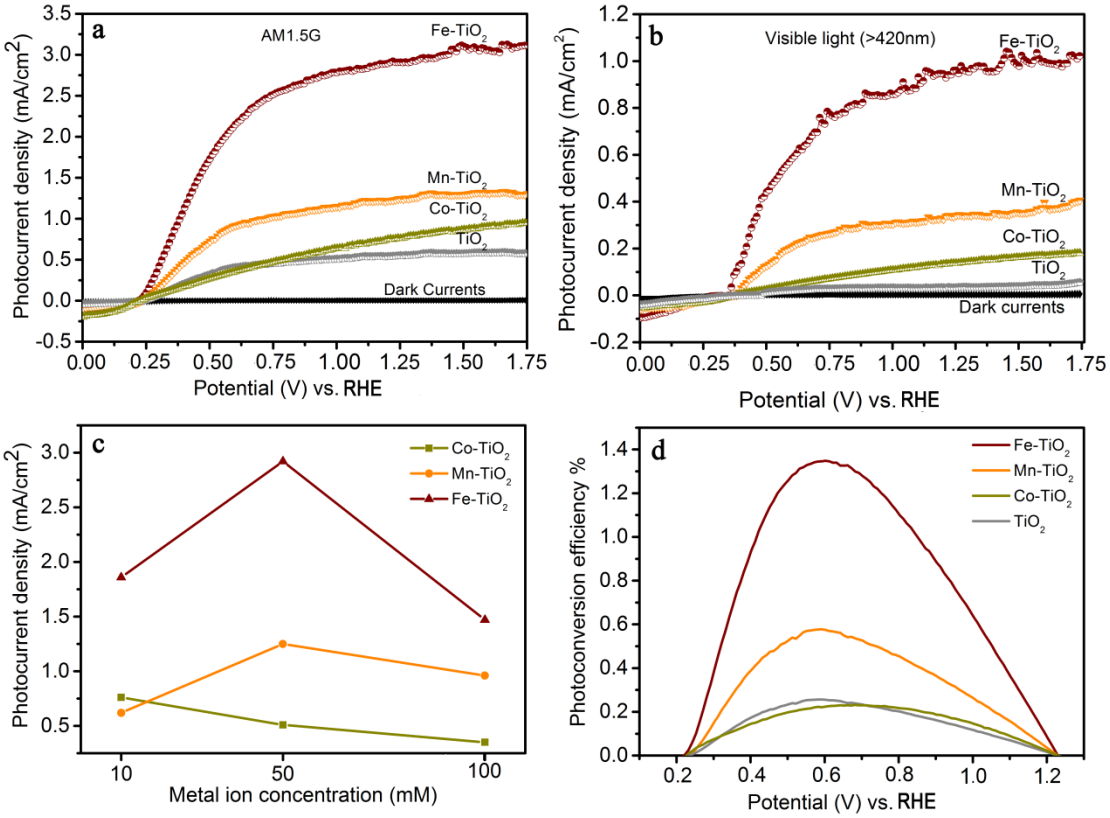


Figure 5. (a,b) Photocurrent density vs applied potential curves of four nanorod photoanodes under AM 1.5G solar illumination (a) and visible light illumination >420nm (b): the $TiO_2$ nanorods (gray curve), the Fe-$TiO_2$ nanorods (wine curve), the Mn-$TiO_2$ nanorods (orange curve), and the Co-TiO2 nanorods (green-yellow curve). The dark currents of the four samples are plotted as a black dotted line for comparison. (c) Photocurrent density vs metal ion concentration at 1.25 V vs RHE. (d) Calculated photoconversion effeciencies for the four samples, as a function of applied potential vs RHE.

To quantitatively determine the conversion efficiency of photon energy to chemical energy from TM doped $TiO_2$ samples, the photoconversion efficiency is calculated based on the equation,[9] $\eta = I\ (1.23 - V)/J_{light}$,

where V is the applied voltage versus reversible hydrogen electrode (RHE), I is the photocurrent density at the measured potential, and $J_{light}$ is the irradiance intensity of 100 mW/cm$^2$ (AM 1.5G). As shown in Figure 5d, the Fe-$TiO_2$ exhibits the highest efficiency of 1.35% at a low bias of 0.6 V vs RHE, the Mn-$TiO_2$ achieves 0.58% at a voltage of 0.6 V vs RHE, and the Co-$TiO_2$ shows 0.24% at 0.7 V vs RHE. Compared to the photoconversion efficiency of 0.26% at 0.6 V vs RHE measured from the undoped $TiO_2$, the Fe doping can significantly increase the maximum photocurrent at a similar saturation potential and greatly improve the photoresponse under visible light, thus leading to a much improved photoconversion efficiency. Although the photocurrent density of Co-$TiO_2$ is higher than that of pure $TiO_2$ especially under visible light illumination, the photoconversion efficiency is slightly lower than that of pure $TiO_2$ due to the high saturation potential.

Considering that the $TiO_2$ nanorods doped with different metal ions exhibit different colors, to further investigate their wavelength-dependent photoelectrochemical properties is important for understanding the interplay between the photocatalytic activity and the light absorption of these samples. IPCE is powerful to quantitatively reveal their photocatalytic activity as a function of wavelength of incident light. We have performed IPCE measurements of the TM-$TiO_2$ nanorod samples at 0.6 V vs RHE, as shown in Figure 6a. IPCE can be expressed by the

following equation,

$$IPCE=(1240I)/(\lambda J_{light})$$

where I is the measured photocurrent density at a specific wavelength, λ is the wavelength of incident light, and $J_{light}$ is the measured irradiance at a specific wavelength. The IPCE values of the Fe-$TiO_2$ nanorod sample increase slowly from almost zero at 560 nm to 3.0% at 500 nm, and then rapidly increase to 15.6% at 430 nm, and finally maintain relatively high efficiencies of 16-18.3% at 300-430 nm. Clearly, the Fe-$TiO_2$ nanorod sample significantly improves the photoresponse not only in UV region but also in the visible light region compared to the undoped $TiO_2$ nanorods. Although the Mn-$TiO_2$ nanorods also exhibit obviously enhanced photoactivity in the visible light region, the IPCE values decrease gradually from 7% at 400 nm to 0.6% at 300 nm. For the Co-$TiO_2$ nanorod sample, the photoresponse is also extended to the visible light region, but the IPCE values are lower than those of $TiO_2$. In the present circumstances, Fe doping is the most effective route to enhance the photoactivity of $TiO_2$.

The IPCE values are relatively low compared to the overall photocurrents. To understand why there is such a discrepancy between the photocurrents and the integration of the IPCE results, the effect of light intensity on the photocurrents of Fe-$TiO_2$ were investigated at an external bias 0.6 V vs. RHE (see in surporting information). Figure S3 shows the

variation of the photocurrents with the incident optical power. In the relatively low power range, the photocurrent is low partly due to the more important contribution of trap recombination. Trap filling can enhance the lifetime of the photogenerated charge carriers and can improve the quantum yield at higher light intensities,[47-49] With increased intensity, the traps can be saturated, leading to enhanced photocurrent. Therefore, We think that the relatively low IPCE values should be attribute to trap filling effect due to weaker light intensity at IPCE measurements.

The optical absorption of TM-doped $TiO_2$ samples was measured to further analyze the contribution for their PEC performance, as shown in Figure 6b. All absorption spectra of the TM-doped $TiO_2$ show an obviously red shift, which can be attributed to the charge transfer transitions between the metal ion d electrons and the $TiO_2$ conduction or valence band. The band gaps of the TM-doped $TiO_2$ and undoped $TiO_2$ estimated by their absorption spectra (see in supporting information Fig. S5) are 2.15 eV (for Fe doped $TiO_2$), 2.17 eV (for Mn doped $TiO_2$), 2.34 eV (for Co doped $TiO_2$), and 3.01 eV (for undoped $TiO_2$), respectively. Although all TM-doped $TiO_2$ samples exhibit a broader and stronger absorption than the undoped $TiO_2$, only the Fe-$TiO_2$ sample achieves the significant enhancement of the PEC performance. Relatively limited improvement for Mn-$TiO_2$ and negligible enhancement for Co-$TiO_2$ probably results from the inefficient separation and transportation of

photoexcited charge carriers.

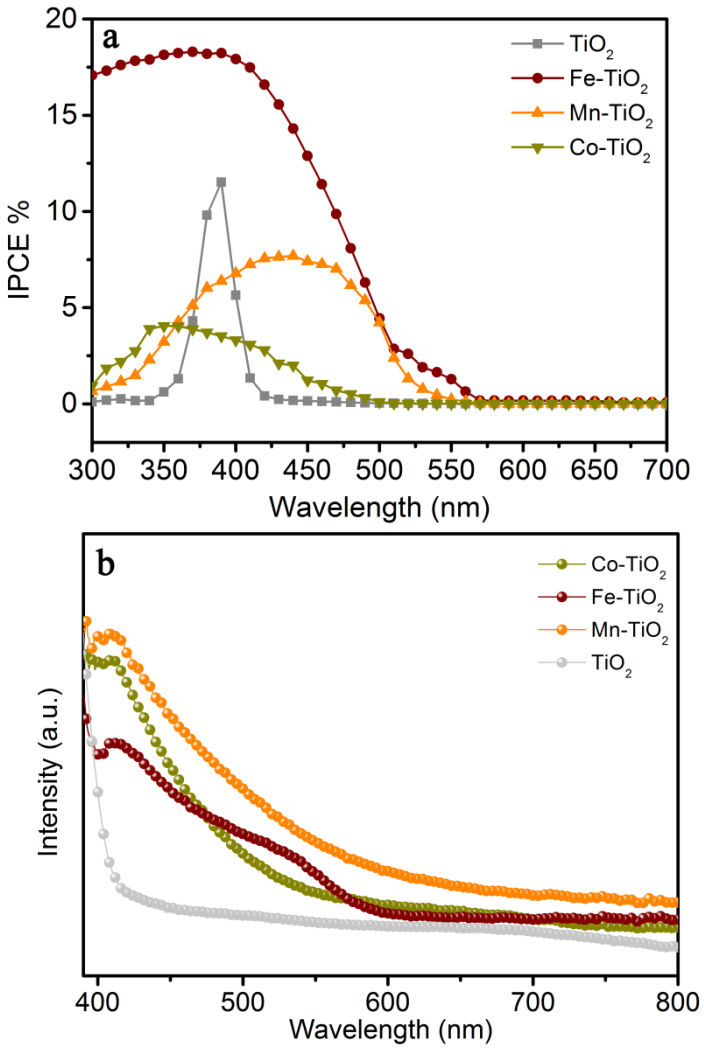


Figure 6. (a) IPCE spectra of the $TiO_2$ (gray), Fe-$TiO_2$ (wine), Mn-$TiO_2$ (orange) and Co-$TiO_2$ (green-yellow) nanorod photoelectrodes measured at an applied bias of 0.6 V (vs RHE) in 1M KOH solution. (b) Optical absorption spectra of the $TiO_2$ (gray), Fe-$TiO_2$ (wine), Mn-$TiO_2$ (orange) and Co-$TiO_2$ (green-yellow) nanorod arrays on the FTO substrates.

To further understand the different PEC performance of the $TiO_2$ nanorods doped with different TM ions, electrochemical impedance spectroscopy measurements were conducted at a frequency of 1 kHz in the dark. The Mott Schottky plots of the undoped and TM doped $TiO_2$ nanorods are displayed in Figure 7. All four $TiO_2$ nanorod samples exhibit

a positive slope in the corresponding Mott Schottky plots, as expected for n-type semiconductor. According to the Mott Schottky equation,

$$1/c^2 = (E - E_{FB} - kT/e)/N_d e\varepsilon_0\varepsilon$$

where $c$ is the space charge capacitance in the semiconductor, $E$ is the applied potential, $E_{FB}$ is the flat band potential, $T$ is the temperature, and $k$ is the Boltzmann constant, $e$ is the elemental charge, $N_d$ is the charge carrier density, and $\varepsilon_0$ and $\varepsilon$ are the vacuum permittivity and the relative permittivity of the $TiO_2$ ($\varepsilon = 170$),[50] respectively. The charge carrier densities ($N_d$) of the $TiO_2$ nanorod samples were calculated from the Mott Schottky plots using the following equation:

$$N_d = 2\left(\frac{dE}{d\left(\frac{1}{c^2}\right)}\right)\Big/(e\varepsilon_0\varepsilon)$$

The calculated carrier densities of the Fe-$TiO_2$, Mn-$TiO_2$, Co-$TiO_2$ and $TiO_2$ nanorods were $2.32\times10^{19}$, $1.81\times10^{18}$, $5.31\times10^{17}$ and $9.12\times10^{18}$ $cm^{-3}$, respectively. Obviously, Fe doping leads to a significant enhancement of carrier density in $TiO_2$. As the donor concentration increases so does the electron concentration in the conduction band, with the Fermi level energy moving closer to the conduction band edge, which facilitates the charge separation at the $TiO_2$/electrolyte interface by increasing the degree of band bending at the $TiO_2$ surface.[33] The effective charge separation and transportation and enhancement of visible light absorption are inferred to be the major reasons for the IPEC improvement

of the Fe-$TiO_2$ nanorods. In addition, both the Mn-$TiO_2$ and the Co-$TiO_2$ samples show a decrease of charge carrier density compared to that of the undoped $TiO_2$ sample. Mn and Co doping probably induces more defects in $TiO_2$ structures than Fe doping, which acts as recombination centers and results in ineffective charge separation and transportation. It may be responsible for the relatively limited PEC performance improvement for Mn-$TiO_2$ and negligible enhancement for Co-$TiO_2$ compared to that of the undoped $TiO_2$.

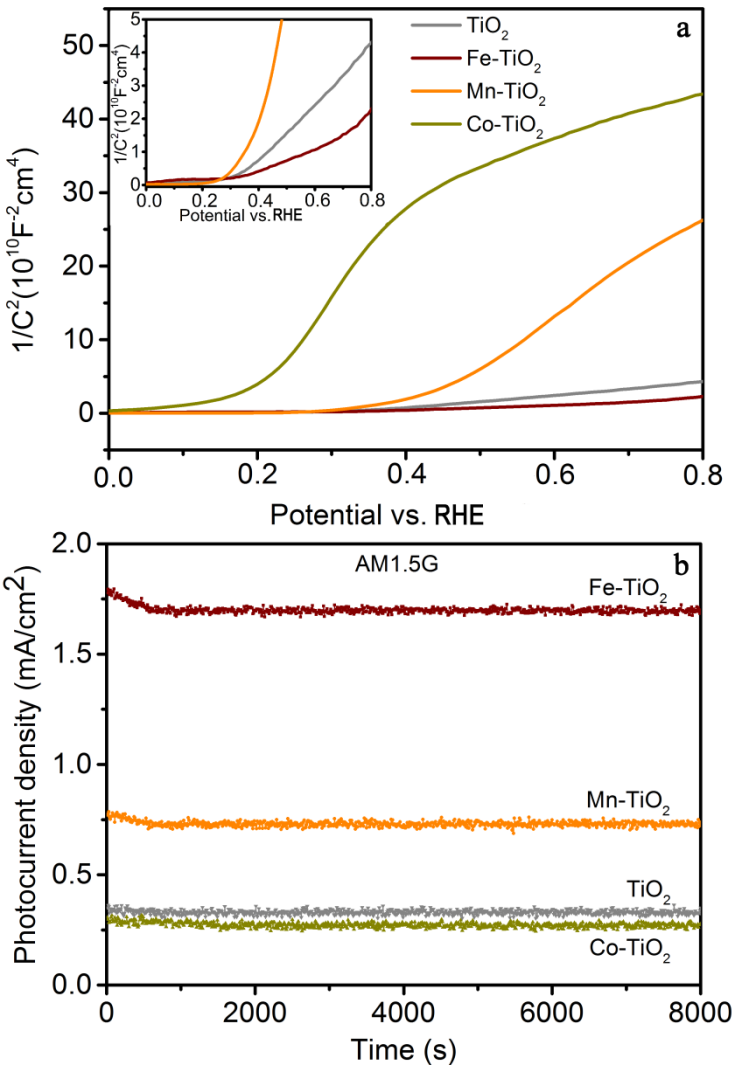


Figure 7. (a) Mott Schottky plots collected at a frequency of 1 kHz in the dark for the Fe-$TiO_2$, Mn-$TiO_2$, Co-$TiO_2$ and $TiO_2$ nanorods. Inset: Mott Schottky plots of the Fe-$TiO_2$, Mn-$TiO_2$ and $TiO_2$

nanorods, measured under the same conditions. (b) Photocurrent densities vs time of the Fe-$TiO_2$, Mn-$TiO_2$, Co-$TiO_2$ and $TiO_2$ nanorods measured at 0.5 V vs RHE under 100 mW/$cm^2$ solar illumination.

To better understand the enhanced PEC performance, the inherent electronic properties of the TM doped $TiO_2$ nanorods were characterized by measuring their open-circuit photovoltage decay (OCPD). OCPD was measured to assess photoelectron lifetime and thus to evaluate the recombination rate of the photoelectrons and holes. OCPD measurement consists of turning off illumination at a steady state and monitoring the subsequent decay of photovoltage, $V_{oc}$, with time (see Fig. S6 in Supporting Information). The $V_{oc}$ decay rate is directly related to the photoelectron lifetime. The calculated photoelectron lifetime is shown in Fig. S7 as a function of $V_{oc}$ (see Supporting Information). Clearly, the photoelectron lifetime increases with decreasing $V_{oc}$. The Fe doped $TiO_2$ nanorods showed relatively long electron lifetime, contributing to it's high PEC performances, in good agreement with the above results. The $TiO_2$ photoanode stability was tested at 0.5 V vs RHE under continuous solar illumination for 8000 seconds (Figure 7b). There is no observable degradation, indicating excellent chemical and structural stability of the TM doped $TiO_2$ nanorods for long-term PEC conversion. We further performed the $O_2$ evolution experiment of Fe-$TiO_2$ sample over a period of 600 min to evaluate its $O_2$ genetation ability and stability (see in surporting information). The Fe-$TiO_2$ photoanode under visible light

illumination exhibited a stable $O_2$ generation ability, as shown in Figure S8. The calculated faradaic efficiency is around 86%.

## 4. Conclusion

We report the first demonstration of transition-metal doping treatment as a facile and effective strategy to substantially improve the performance of $TiO_2$ nanorods for photoelectrochemical (PEC) water splitting. The effect of Fe, Mn and Co as dopants on the PEC performance of the $TiO_2$ nanorods were investigated in which the Fe doping is the most effective route to enhance the photoactivity of $TiO_2$. The photocurrent density of Fe-$TiO_2$ sample increases significantly with bias voltage and reaches 2.92 $mA/cm^2$ at 1.25 V vs RHE, which are five times higher than that of the undoped $TiO_2$. Even under visible light illumination (>420 nm), the photocurrent density of Fe-$TiO_2$ is as high as 0.96 $mA/cm^2$ at 1.25 V vs RHE. Incident-photon-to-current-conversion efficiency (up to ~ 18%) measurements reveal that the Fe-$TiO_2$ nanorod sample significantly improves the photoresponse not only in the UV region but also in the visible light region. Fe dopants not only enhance visible light absorption of $TiO_2$ nanorods by creating impurity energy levels near the conduction band, but also obviously increase carrier density of $TiO_2$, leading to effective carrier separation and transportation and relatively long electron lifetime. Due to their relatively high photocatalytic activity, Fe-$TiO_2$

nanorods can serve as a promising candidate for various areas, such as solar water splitting, dye-sensitized solar cells, and photocatalysis.

## Acknowledgments

This work was financially supported by the National Natural Science Foundation of China (Grant No. 51102017).

## References

(1) Hoffmann, M. R.; Martin, S. T.; Choi, W.; Bahnemann, D. W. Chem. Rev., 1995, 95, 69–96.
(2) Grätzel, M. Nature 2001, 414, 338–344.
(3) C. X. Kronawitter, L. Vayssieres, S. Shen, L. Guo, D. A. Wheeler, J. Z. Zhang, B. R. Antoun and S. S. Mao Energy Environ. Sci., 2011, 4, 3889.
(4) Asahi, R.; Morikawa, T.; Ohwaki, T.; Aoki, K.; Taga, Y. Science, 2001, 293, 269−271.
(5) M. R. Shaner, K. T. Fountaine, S. Ardo, R. H. Coridan,H. A. Atwater and N. S. Lewis Energy Environ. Sci., 2014, 7, 779–790.
(6) Maeda, K.; Teramura, K.; Lu, D.; Takata, T.; Saito, N.; Inoue, Y.; Domen, K.; Nature 2006, 440, 295.
(7) Tada, H.; Mitsui, T.; Kiyonaga, T.; Akita, T.; Tanaka, K. Nat. Mater. 2006, 5, 782-786.
(8) J. Sun, D. K. Zhong and D. R. Gamelin Energy Environ. Sci., 2010, 3, 1252–1261.
(9) Walter, M. G.; Warren, E. L.; McKone, J. R.; Boettcher, S. W.; Mi Q.; Santori, E. A.; Lewis, N. S.; *Chem. Rev.*, 2010, 110, 6446–6473.
(10) Chen, X.; Shen, S.; Guo, L.; Mao, S. S. Chem. Rev., 2010, 110, 6503–6570.
(11) Hensel, J.; Wang, G.; Li, Y.; Zhang, J. Z. Nano Lett. 2010, 10, 478-483.
(12) Amirav, L.; Alivisatos, A. P. J. Phys. Chem. Lett. 2010, 1, 1051–1054.
(13) Paracchino, A.; Laporte, V.; Sivula, K.; Grätzel, M.; Thimsen, E., Nat. Mater. 2011, 10,

456-461.
(14) Chen, X.; Liu, L.; Yu, P. Y.; Mao, S. S. Science, 2011, 331, 746−750.
(15) M. Liu, L. Wang, G. Lu, X. Yao and L. Guo Energy Environ. Sci., 2011, 4, 1372.
(16) Sun, J.; Liu, C.; Yang, P. J. Am. Chem. Soc. 2011, 133, 19306–19309.
(17) Seh, Z. W.; Liu, S.; Zhang, S.-Y.; Bharathi, M. S.; Ramanarayan, H.; Low, M.; Shah, K. W.; Zhang, Y.-W.; Han, M.-Y. Angew. Chem. Int. Ed. 2011, 50, 10140–10143.
(18) Seh, Z. W.; Liu, S.; Low, M.; Zhang, S.-Y.; Liu, Z.; Mlayah, A.; Han, M.-Y.; Adv. Mater. 2012, 24, 2310-2314.
(19) Abdi, F. F.; Han, L.; Smets, A. H.M.; Zeman, M.; Dam, B.; van de Krol, R. Nat. Commun. 2013, 4, 2195.
(20) Seger, B.; Pedersen, T.; Laursen, A. B.; Vesborg, P. C. K.; Hansen, O.; Chorkendorff, I. J. Am. Chem. Soc. 2013, 135, 1057−1064.
(21) Liu, C.; Tang, J.; Chen, H. M.; Liu, B. Yang, P. Nano Lett. 2013,13,2989-2992.
(22) Fujishima, A.; Honda, K. Nature 1972, 238, 37.
(23) Chen, X.; Mao, S. S. Chem. Rev., 2007, 107, 2891–2959.
(24) Umebayashi, T.; Yamaki, T.; Itoh, H.; Asai, K. J. Phys. Chem. Solids 2002, 63, 1909.
(25) Shao, G. J. Phys. Chem. C 2008, 112, 18677–18685.
(26) Liu, S.; Guo, E.; Yin, L. J. Mater. Chem., 2012, 22, 5031.
(27) Su, R.; Bechstein, R.; Kibsgaard, J.; Vang, R. T.; Besenbacher, F. J. Mater. Chem., 2012, 22, 23755.
(28) Peng, B.; Meng, X.; Tang, F.; Ren, X.; Chen, D.; Ren, J. J. Phys. Chem. C 2009, 113, 20240–20245.
(29) Choi, J.; Park, H.; Hoffmann, M. R. J. Phys. Chem. C 2010, 114, 783–792.
(30) Mor, G. K.; Varghese, O. K.; Wilke, R. H. T.; Sharma, S.; Shankar, K.; Latempa, T. J.; Choi, K.; Grimes, C. A. Nano Lett. 2008, 8, 1906-1911.
(31) Hoang, S.; Guo, S.; Hahn, N. T.; Bard, A. J.; Mullins, C. B. Nano Lett. 2012, 12, 26−32.
(32) Hoang, S.; Berglund, S. P.; Hahn, N. T.; Bard, A. J.; C. Mullins, B. J. Am. Chem. Soc. 2012, 134, 3659−3662.
(33) Wang, G.; Wang, H.; Ling, Y.; Tang, Y.; Yang, X.; Fitzmorris, R. C.Wang, C.; Zhang, J. Z.; Li, Y. Nano Lett. 2011, 11, 3026–3033.
(34) Xu, M.; Da, P.; Wu, H.; Zhao, D.; Zheng G. Nano Lett. 2012, 12, 1503−1508.
(35) Hwang, Y. J.; Hahn, C.; Liu, B.; Yang, P. D. ACS Nano 2012, 6, 5060–5069.
(36) Cho, I. S.; Chen, Z.; Forman, A. J.; Kim, D. R.; Rao, P. M.; Jaramillo, T. F.; Zheng, X. Nano Lett. 2011, 11, 4978–4984.
(37) Mor, G. K.; Prakasam, H. E.; Varghese, O. K.; Shankar, K.; Grimes, C. A. Nano Lett. 2007, 7, 2356–2364.
(38) Wang, Y.; Zhang, Y. Y.; Tang, J.; Wu, H.; Xu, M.; Peng, Z.; Gong, X. G.; Zheng, G. ACS Nano 2013, 7, 9375–9383.
(39) Liu, B.; Aydil, E. S. J. Am. Chem. Soc. 2009, 131, 3985–3990.
(40) Chen, X.; Liu, L.; Yu, P. Y.; Mao, S. S. Science 2011, 331,746–750.
(41) Lazarus, M. S.; Sham,T.K. Chem. Phys. Lett. 1982, 92, 670–673.
(42) Allen, G. C.; Harris, S. J.; Jutson, J. A.; Dyke, J. M. Appl. Surf. Sci. 1989, 37, 111.
(43) Chen, A. J.; Wu, X. M.; Sha, Z. D.; Zhuge, L. J.; Meng, Y. D. J. Phys. D: Appl. Phys. 2006, 39, 4762.

(44) Bonnelle, J.P.; Grimblot, J.; D'huysser, A. J. Electron Spectrosc. Relat. Phenom. 1975, 7, 151.
(45) Kim, K.S. Phys. Rev. B 1975, 11, 2177.
(46) Liu, M. Z.; Snapp, N. D.; Park, H. Chem. Sci. 2011, 2, 80–87.
(47) E. Fabre, M. Mautref, and A. Mircea, Appt. Phys. Lett. 1975, 27, 239.
(48) C. F. Ho, R. O. Bell, and F. V. Wald, Appl. Phys. Lett. 1977, 31, 463.
(49) R. Pandya and E. A. Schiff, Philosophical Magazine B, 1985, 5 2, 1075-1095.
(50) Parker, R. A. Phys. Rev. 1961, 124, 1719–1722.